MALAYSIAN JOURNAL OF MICROSCOPY

Journal homepage: https://malaysianjournalofmicroscopy.org

RESEARCH ARTICLE

EFFECT OF SURFACE LASER SHOCK PEENING ON THE TENSILE PROPERTIES AND HARDNESS OF SELECTIVE LASER MELTED (SLMed) A357 ALLOY

Agbaye Ignatius Uyabemem[1,2], Tuty Asma Abu Bakar[2,3,*], Aini Zuhra Abdul Kadir[3]

[1]Department of Metalworks Technology Education, School of Technical Education, Federal College of Education (Technical), Asaba, Delta State, Nigeria.
[2]Materials Research and Consultancy Group (MRCG), Department of Mechanical Engineering, Faculty of Mechanical Engineering, Universiti Teknologi Malaysia, 81310 Johor Bahru, Malaysia.
[3]Department of Materials and Industrial Engineering, Faculty of Mechanical Engineering, Universiti Teknologi Malaysia, 81310 Johor Bahru, Malaysia.

Abstract. Selective laser melting (SLM) has been widely used to fabricate Al-Si-Mg alloys, which are extensively used in the automotive, aerospace, and biomedical industries. However, due to its rapid solidification and cooling rates, the process induces thermal fluctuations that lead to residual stresses in the parts, necessitating stress-relief post-processing. This study examines the influence of surface laser shock peening (LSP) on the residual stress profile, microstructure, hardness and tensile properties of A357 alloy fabricated by SLM. LSP treatment was done using controlled laser parameters and dimple spacing. X-ray diffraction analysis shows that compressive residual stresses up to -57 MPa were produced, which modified the tensile residual stresses (TRS). Variable pressure scanning electron microscopy (VP-SEM) revealed remarkable grain refinement and a uniform distribution of primary α-Al and fibrous Si phases after LSP, which is attributed to LSP-induced plastic deformation and a high dislocation density. This produced an improvement of about 18.6 % in hardness. Mechanical tests recorded improvement in strength, as yield strength (YS) increased from 87±0.87 to 155±1.32 MPa, about 78 % increase, while ultimate tensile strength (UTS) increased from 197±1.0 MPa to 263±3.61 MPa, representing 33.4 % increase at the bottom of the sample. At the sample top, YS increased from 95±1.0 MPa to 171±2.65 MPa, a 80 % increase, while the UTS increased from 200±2.65 MPa to 269±2.65 MPa, representing 34.5 % increase. However, elongation decreased slightly due to strain hardening. Analysis of fractured surfaces reveals reduced porosity and defect closure in the LSP-treated samples, which inhibited crack initiation and propagation. This confirms that LSP is an effective strategy for mitigating residual stresses and improving the mechanical performance of the A357 alloy, making it appropriate for critical structural applications.

Keywords: Laser shock peening, selective laser melting, residual stress, aluminium alloys.

Article Info

Received 10 January 2026
Accepted 12 May 2026
Published 8 June 2026

***Corresponding author: tuty@utm.my**

ISSN: 1823-7010, eISSN: 2600-7444

1. INTRODUCTION

Aluminium A357, also known as AlSi7Mg, finds extensive application in automotive, aerospace, and biomedical structures because of its unique combination of high specific strength, low density, good corrosion resistance, and castability [1, 2]. In the heat-treated state, A357 exhibits remarkable ultimate tensile strength (UTS) and yield strength (YS) of 360 MPa and 297 MPa, respectively, with appreciable hardness, making it useful for industrial applications [3-5] A357, because of lower Silicon (Si) content, has better ductility, toughness and fatigue life compared to AlSi10Mg, which is more brittle due to higher Si content [6-8] A357 alloys have been fabricated through conventional casting methods [9, 10]. The materials produced by these methods are known to have coarse grains and defects such as shrinkage cavities, porosity, and inclusions [4], which affect the mechanical properties.

Selective Laser Melting (SLM), an additive manufacturing (AM) process, owing to its rapid solidification, produces alloys with ultrafine microstructures, high densification, and low porosity compared to casting methods. Therefore, achieving better mechanical properties [1,11]**.** However, despite the impeccable benefits of SLM, the repeated thermal cycles in layer-by-layer deposition and the rapid solidification process produce tensile residual stresses (TRS), which can lead to warping, poor dimensional accuracy, and cracking, increasing the risk of material distortion and premature failure [12-14].

Some researchers have made efforts to characterise the residual stresses in Selective laser melted (SLMed) alloys, and have employed several measures to mitigate them. Chen et al. [15] found that SLMed samples with higher surface roughness exhibited low residual stresses. This study opened the door to shot peening as a post-processing method to mitigate residual stresses. But increasing surface roughness also creates crack-initiation sites, which affect the important mechanical properties of the parts, such as fatigue resistance and fracture toughness [16]. Unlike shot-peening, in which a hard ball is mechanically dropped onto the sample surface, laser shock-peening (LSP) uses a high-energy laser that passes through a thin layer of water to generate a pressure wave that penetrates the sample, creating compressive residual stresses (CRS).

Kalentics et al. [17] found that LSP converted TRS to CRS. They reported that using small spot sizes results in a higher magnitude of CRS at the surface, while larger spot sizes give deeper CRS penetration in LSP austenitic steel. Sandmann et al. [18] with LSP obtained about -300 to -400 MPa, which modified TRS in LPBF fabricated 316L stainless steel. Ramadas et al. [19] also obtained a CRS up to -800 MPa after LSP, which improved the yield strength, ultimate tensile strength, and elongation of LPBF-made stainless steel. They attributed it to microstructural refinement, increased LAGBs and dislocation density. On Al-Si alloys, Vemanaboina et al. [20] recorded CRS of about -80 MPa and -104 MPa along the length and face of SLMed AlSi10Mg solid cylinder, using X-ray diffraction (XRD) analyser. Nasab et al. [12] studied the effect of laser shock-peening (LSP) on the fatigue life of AlSi10Mg produced via SLM, and reported 50 % improvement in the fatigue properties of the alloy after LSP.

Despite the growing body of literature on residual stress characterisation and mitigation in structural materials, there is less work on A357 fabricated via SLM, particularly on the use of LSP post-processing to mitigate residual stresses. Before 2018, there were no published studies on the LSP of SLMed A357 until Hatamleh [21-23] conducted studies using finite element modelling (FEM) to propose a reliability-based design for the LSP treatment of SLMed A357. Ever since then, there has been no practical deployment of LSP to mitigate residual stresses in SLMed A357 alloys.

This study measures the residual stresses in A357 produced by SLM, and carries out laser shock peening (LSP) post-processing treatment, with controlled spot size and dimples spacing, using the robotic X-ray diffraction and *pulstec* machines. Mechanical tests were conducted to determine the strength and hardness of the as-printed and LSP-treated samples and to evaluate LSP's effectiveness in improving the mechanical properties required for aerospace and biomedical applications.

2. MATERIALS AND METHODS

2.1 Selective Laser Melting

All the A357 samples were fabricated using the SLM machine (EOS M290) from 99.9 % purity powder with an average particle size of 45 µm. The chemical composition of the A357 material is as shown in Table 1. The process parameters used in the SLM fabrication process are shown in Table 2. Six samples were printed on an aluminium 5083 substrate plate, and built into rectangular-shaped bars with a cross-sectional area of (127 mm x 6.35 mm x 12.8 mm) as shown in Figure 1.

Table 1: Chemical composition (wt.%) of A357 aluminium alloy

Element	Composition (wt.%)
Silicon (Si)	7.0
Iron (Fe)	0.2
Copper (Cu)	0.2
Manganese (Mn)	0.1
Magnesium (Mg)	0.4
Titanium (Ti)	0.04
Zinc (Zn)	0.1
others	0.6
Aluminium (Al)	88.36

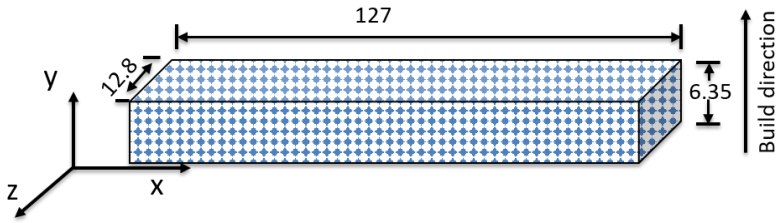

Figure 1: SLM built rectangular block sample with dimensions in (mm)

The energy per unit volume of powder deposited, also known as volumetric energy density, can be calculated by the ratio of the power (W) to the product of the scan speed (υ), hatch spacing (*h*), and powder layer thickness (t) according to Equation 1.

$$VED = \frac{P}{\upsilon \, x \, h \, x \, t} \tag{1}$$

Based on the process parameters used to print the samples shown in Table 2, the VED was determined to be 43.15 J/mm^3. This energy is moderate, and neither too high nor too low, which completely avoids extreme melt pool, risk of keyhole formation, splatter, lack of fusion porosity, and incomplete melting in the case of low VED.

Table 2: SLM process parameters

Process Parameter	Laser power (W)	Scan speed (mm/s)	Hatch spacing (mm)	Layer thickness (µm)
Selected Values	290	1200	0.14	40

2.2 Residual Stress Measurement

2.2.1 LSP Sample Measurement

The "KUKA" robotic X-ray machine with a Cu radiation tube was used to measure stress in the LSP sample. The material/diffraction plane/angle was set to Al (422) 135.7 °, and the collimator size was 11.95 mm, with voltage and current of 30 kV and 10 mA, respectively. The laser exposure time was 15 s, the number of tilts was 5, and the tilt angle ranged from -45 ° to 45 °. The samples were mapped into three equal parts on both positive and negative movement of the laser head, as shown in Figure 2(b). A total of 75 dimples were measured, similar to the hardness test mapping, but residual stress measurements were performed before hardness testing.

2.2.2 Hardness Testing and Microstructural Characterisation

The vicker's hardness measurements for both the as-printed and LSP samples were performed with the Struers Dura Scan (Model 80 DURASCAN-70) machine, with optical lens magnification 40x and pressure of Hv0.1, and a hold time of 10 s at room temperature. A total of 75 points (Pts) were mapped on the sample, with P_1(x = 0, y = 0), P_2 (x = 0, y = 200 µm), P_3 (x = 0, y = -200 µm), up to P_L (x_L = 25 mm, y = -200 µm). P_L is the last point (75^{th}), and x_L is the last distance along the x-axis on the sample surface, as shown in Figure 2(b). The indentation distances were in accordance with the ISO 6507-7 recommendation. Three parallel rows, each having 25 indentations separated by 200 µm, and the average microhardness is plotted. The microstructural feature was determined using a variable pressure scanning electron microscope (VP-SEM) JSM-IT300 equipped with a Bruker Energy-dispersive X-ray spectroscopy (EDS) detector.

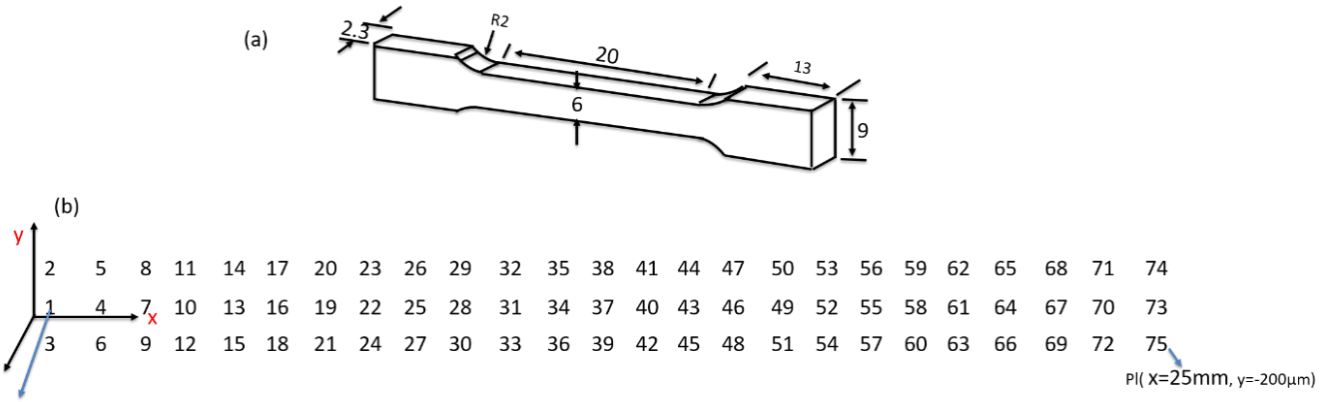

Figure 2: Schematics showing (a) Geometry and configuration of the tensile test samples and (b) Indent distance coordinates mapping for the microhardness of the samples

2.2.3 As-printed Sample Measurement

The measurement of residual stress in the as-printed sample was carried out with *a "Pulstec"* X-ray residual stress machine equipped with u360 software, after the robotic machine developed an uncertainty issue and could not be calibrated. Unlike the *Kuka* robotic X-ray device, the *Pulstec* machine has an easy set-up; it does not need calibration or collimator setting, as the distance between the beam detector and the sample is automatically set at 40 mm. The material type, diffraction plane, and sample distance from the detector were set to Aluminium (311), 40 mm, and 30 °, respectively.

In XRD residual stress measurements, the uncertainty level is critical, as it reflects how the measured value deviates from the true value. The Kuka robotic machine has an uncertainty level of

about ±0.05 mm, which shows the pose repeatability, or how the robot can return to the same position repeatedly. This depends on the friction, robotic joint tolerances, collimator settings, etc. If these are not well measured and properly managed, they contribute to spatial uncertainty and affect the accuracy of the results. Prior to the measurement, the collimator was set at 11.95 mm, and the robot's tool centre point (TCP) was precisely calibrated before commencing measurement. In addition, the experiment was conducted in an air-conditioned room with the temperature maintained at 16 °C, ensuring that no noise or vibration approached the room. Finally, the measurements were repeatedly done to estimate and reduce the combined uncertainty. For the Pulstec XRD machine, uncertainty may arise from detector noise, the collimator, sample conditions, etc., and can also affect the accuracy of the measured stress. The designers took precautions by making the device with a fixed collimator distance (40 mm). However, care was taken to carry out the experiment in the same temperature-controlled, noise and vibration-free environment.

2.3 Laser Shock Peening

The working principles of the LSP is illustrated by the schematic in Figure 3(a). The LSP treatment was performed with an Nd:YAG laser machine with 1064 nm wavelength, operating at pulse duration of 6.5 ns. Based on parameters for the LSP of similar metals [12,21]. The frequency was set to 10 Hz, and the pulse profile's Full Width at Half Maximum was 17 ns. A deionised laminar water film was used as the transparent overlay to maximise plasma duration and the intensity of the generated pressure. The laser spot shape was circular, with a 2 mm focus diameter. The laser energy used was 8 J/pulse, with a laser intensity of 7.9 GW/cm^2. A graphite coating was applied to the sample's surface to maximise compressive residual stress and protect against surface damage. The LSP surface consisted of 4 rows, each with 25 dimples, for a total of 100 dimples with about 50 % overlap. The laser made a single pass through a linear pattern as illustrated in Figure 3(b).

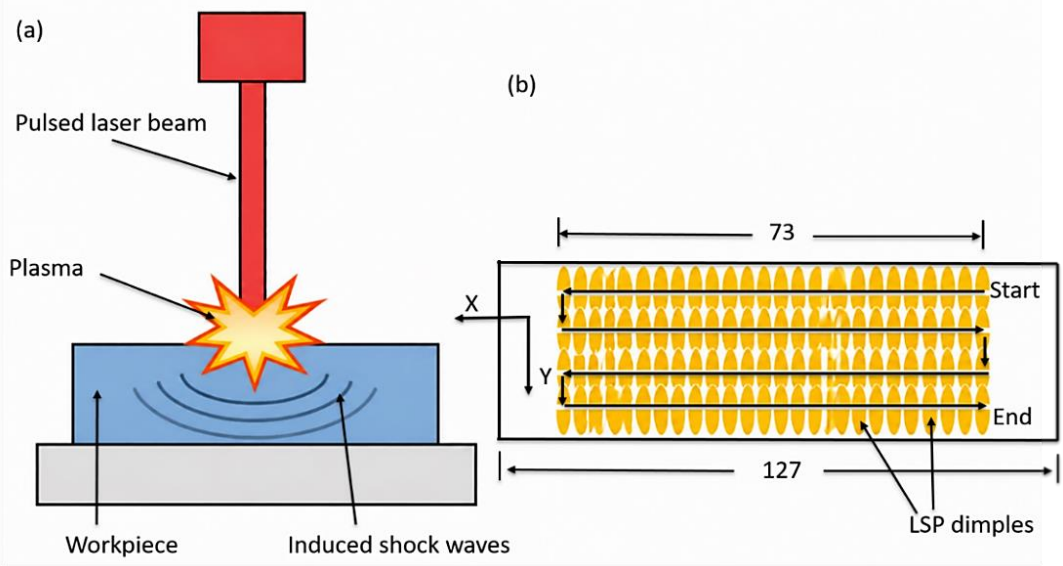

Figure 3: Laser shock peening process showing (a) Schematic of LSP process and (b) Laser travelling pattern in the LSP process.

2.4 Tensile Testing

Three specimens for each case (As-printed and LSP-treated) were wire-cut into dog-bone shapes according to the ASTM E8-3a standard for sub-size samples. The tensile test was performed with the INSTRON 5982 universal tester, operating with '***Instron Bluehill'*** software. The test was carried out at room temperature using a 50 kN load and a constant crosshead speed of 0.2 mm/min. The reason for the

low speed is to minimise localised stress concentrations around brittle Si phases, and allow for uniform plastic deformation. Each test was performed three times to ensure reliability. The tensile samples configuration is shown in Figure 2(a).

3. RESULTS AND DISCUSSION

3.1 Residual stress measurement in as-printed (AP) and LSP samples

Figure 4 shows the development of residual stress measured across the dimples in the LSP sample, as well as the points and their magnitudes at various penetration depths. In line with expectations, tensile residual stresses (TRS) were recorded at the surfaces of the As-printed samples, attributable to the SLM process, characterised by rapid solidification of the melt pool and attendant shrinkage. In the As-printed sample, points 33, 34, 38, and 39 exhibited similar residual stresses, with relatively low compressive stresses in the LSP samples. These could be points of lower scanning speed, which create lower cooling rates, thereby enhancing even shrinkage patterns during the solidification of the printed material [11]. The stress values recorded in the LSP sample indicate that the shock waves generated by the LSP process on the sample surfaces induce CRS from the surface to the material depth, suppressing the TRS. The CRS decreases in value as the shock waves propagate through the bulk material. The CRS has the highest value at the surface (-57 MPa), at 0.05 mm (-51 MPa), and at 0.1 mm (-47 MPa), etc. This could be attributed to regions with lower surface and subsurface porosity, which enhance the absorption and transmission of a substantial amount of LSP energy, thereby increasing the effect of the LSP process [24].

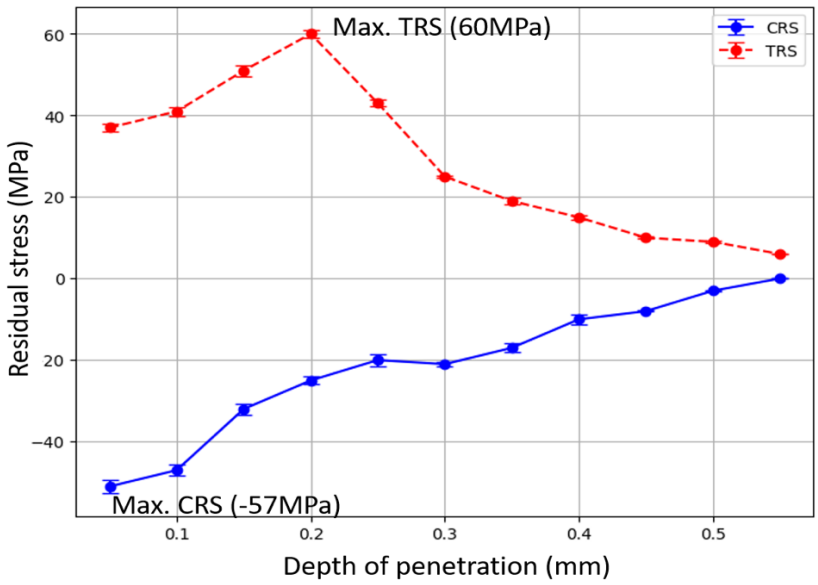

Figure 4: Residual stress in As-printed and LSP A357 samples

3.2 Microhardness properties and microstructure evolution

Figure 5 shows the microhardness recorded for the As-printed sample, the LSP sample at the surface (LSP TOP) and LSP BOTTOM at 1 mm depth in the ZX plane. The XY-plane on the sample is the side face perpendicular to the build direction, while the ZX-plane is the top face parallel to the build direction (Figure 1). It is evident that the plastic deformation-induced strain hardening from the LSP resulted in a slight increase in the hardness of the A357 alloy, to about 22.8 %, at the sample top [19]. It is also observed that the microhardness slightly decreased with increasing thickness of the LSP A357 sample (1 mm thick), confirming that the effect of shock peening decreases from the surface into the bulk of the part [25]. Figure 6 shows the microstructure of the samples in the as-printed state and after

LSP. Figure 6(a) shows the SEM image of the As-printed A357 sample, which clearly reveals the characteristic cellular primary α-Al dendrites, and coarse, irregular fibrous Si cells that grow into an elongated shape towards the build direction, following the solidification path [26]. However, from Figure 6(b), after LSP, fine cellular microstructure is observed with more evenly distributed primary α-Al dendrites, and fibrous fine cellular Si morphology [27]. The average grain size decreased to ~0.51 µm from ~0.82 µm in the as-printed state. This increased the dislocation density, which acts as a barrier to dislocation motion, thereby increasing the alloy's strength and hardness.

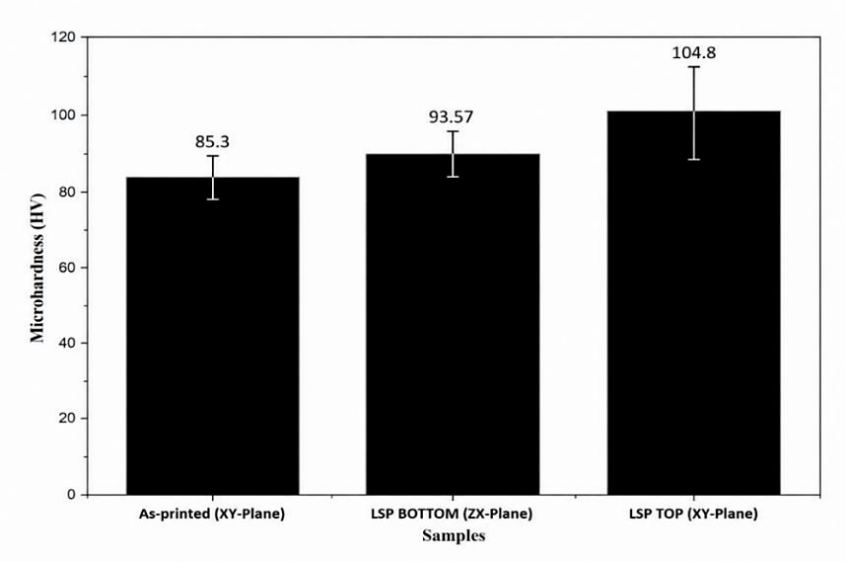

Figure 5: Plot of hardness values of As-printed and LSP Samples

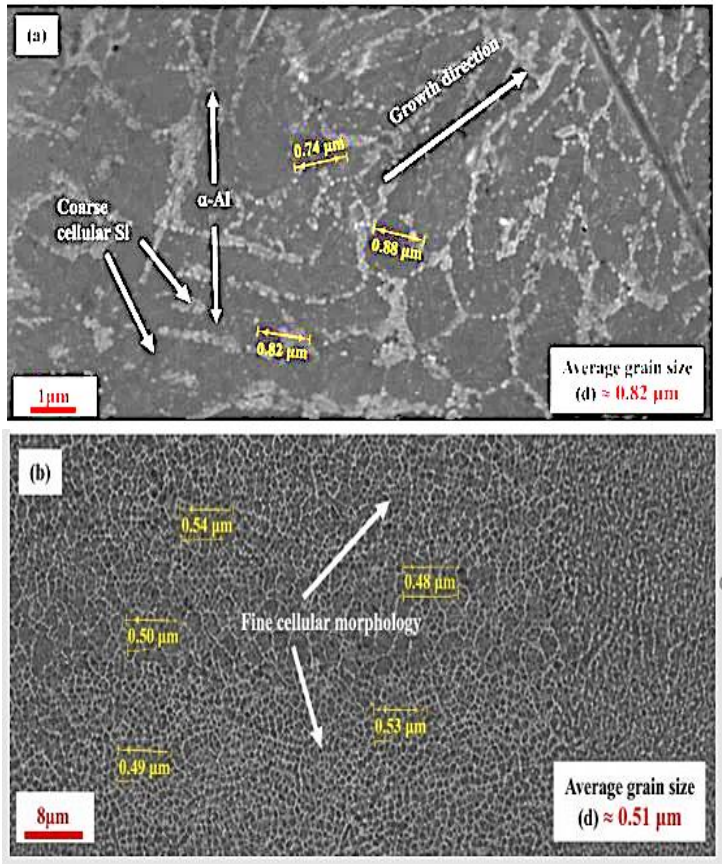

Figure 6: SEM images of (a) As-printed A357 sample and (b) LSP A357 sample

3.3 Tensile test

Figure 7 shows the tensile stress-strain curves of As-printed and LSP A357 samples, with the results tabulated in Table 3. The as-printed BOTTOM sample exhibited the lowest UTS and YS, having values of 197±1.0 and 87±0.87 MPa, respectively. The tensile elongation (TE) was highest in the as-printed BOTTOM sample, being 15±0.781 %. At the top of the as-printed sample (Figure 7(b)), both UTS and YS increased to 269±2.65 MPa and 171±2.65 MPa, respectively, while the TE decreased to 14.2±0.78 %. This is attributed to higher strain hardening in the top region of the samples, due to faster cooling rates and less reheating at the surface than at the bottom [26]. For the top sample, YS increased by about 80 %, while UTS increased by 34.5 %. The bottom sample witnessed 78 % increase in YS, and 33.4 % increase in UTS. This is attributed to LSP-induced CRS, which modified the tensile residual stress (TRS) and enhanced the alloy's strength. It affirms the potential of LSP to modify the residual stress and improve the mechanical properties of SLM-fabricated alloys [12]. The subdivided grains increase dislocation density, which serves as a barrier to dislocation slip [28], leading to improved hardness and strength at the near-surface. The α-Al dendritic network created by the plastic strain deformation also closes some of the near-surface SLM defects such as pores, keyholes and microcracks as evidenced in Figure 9(b), which reduced crack initiation and improved the strength and hardness of the material. However, despite the improvement in strength recorded in this study, it remains lower than that reported in the literature for the as-printed state [11]. This could be attributed to the influence of SLM parameters and process defects such as unmelted powder, pores, and voids, as evidenced in Figure 8.

Table 3: Mechanical properties of tensile test for as-printed and LSP samples

Sample	Y.S-0.2%Ɛ (MPa)	UTS.(MPa)	Modulus of Elasticity (GPa)	Elongation (%)
As-printed TOP	95±1.0	200±2.65	72	14.2±0.75
As-printed BOTTOM	87±0.87	197±1.0	72	15.1±0.781
LSP TOP	171±2.65	269±2.65	72	12.03±0.102
LSP BOTTOM	155±1.32	263±3.61	72	13.37±0.549

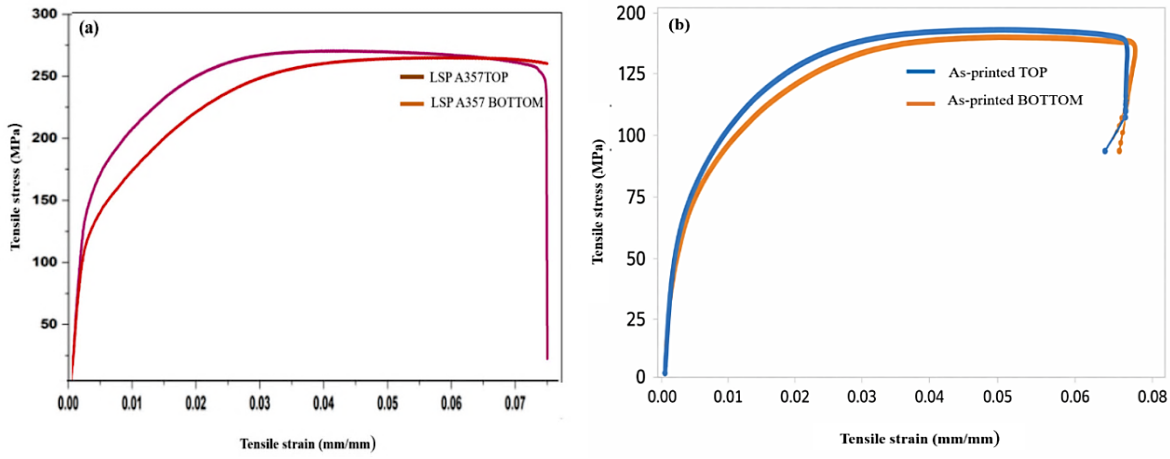

(a) (b)

Figure 7: Tensile stress-strain curves for (a) LSP A357 TOP and LSP A357 BOTTOM and (b) As-printed A357 TOP and As-printed A357 BOTTOM

3.4 Fractography

The SEM image of the fractured surfaces of the tensile specimen for as-printed TOP (Figure 8(a)) reveals cleavage spots of unmelted powder, indicating defects in the SLM process parameters and a lack of fusion. Cleavage facets were also prevalent in the as-printed sample (Figure 8(a)), indicating trans-granular mode crack growth, which indicates signs of brittle fracture. This is attributed to the fracture of primary silicon particles along the Si-Al interface [29]. Figure 8(d) shows that crack propagation developed from surface voids and sub-surface cavities, which grow until final fracture at the region of white dotted lines.

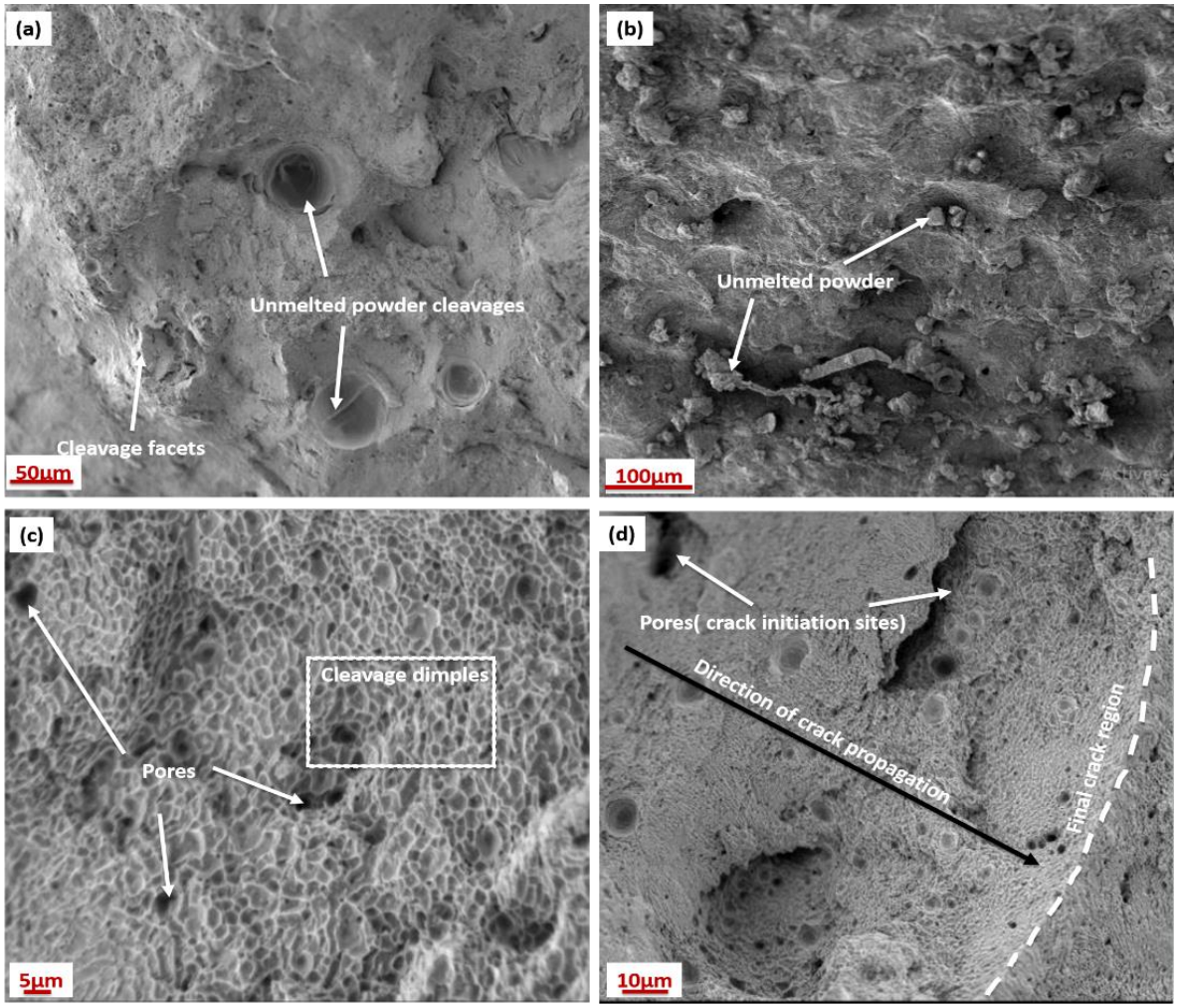

Figure 8: Fracture surface analysis of A357 produced by SLM for (a) As-printed sample at 50 µm, (b) LSP sample at 100 µm, (c) LSP TOP sample at 5 µm and (d) LSP BOTTOM sample at 10 µm

Figure 8(c) shows cleavage dimples in the LSP BOTTOM sample viewed at 5 µm. This accounts for the higher ductility of 13.37±0.549 compared to the LSP TOP, where TE is 12.03±0.102. Nucleated pores dominated the as-printed TOP sample (Figure 9(a)), which remarkably reduced after LSP, as shown in Figure 9(b). This is surface modification by LSP-induced CRS, which creates plastic flow near the surface that heals the sample surface by closing pores and surface defects connected to it, thereby contributing to the 22.8 % improvement in hardness [30].

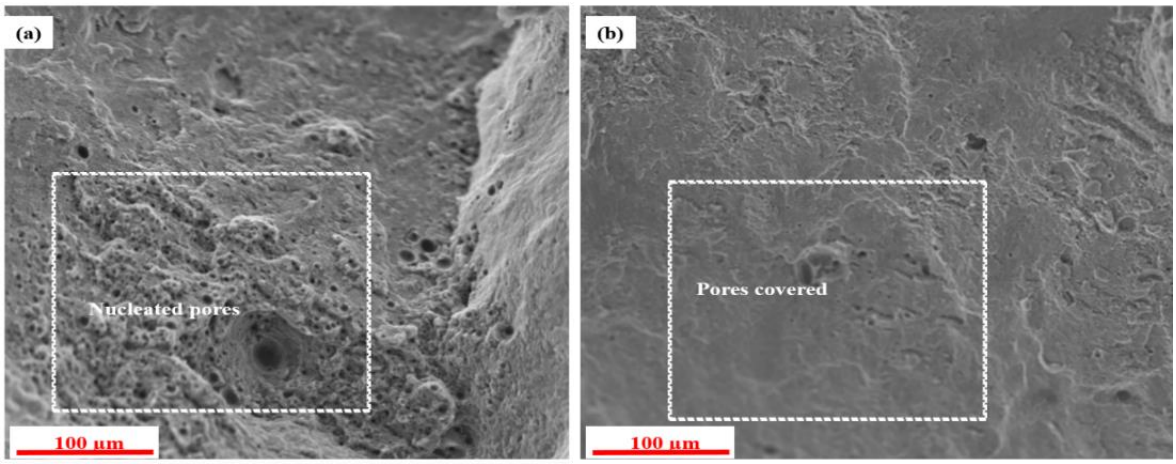

Figure 9: SEM images of fractured surfaces showing (a) nucleated porosity in as-printed TOP sample and (b) Porosity distribution in LSP TOP sample

4. CONCLUSION

The effects of LSP treatment on the microhardness, tensile strength, and microstructure of A357 alloy samples fabricated by SLM were examined. The results reveal that LSP post-processing treatment remarkably improved the alloy's properties by inducing CRS at the sample surfaces, thereby modifying the tensile residual stresses (TRS). The formation of plasma waves induces CRS in the SLMed A357 part up to -57 MPa, which was instrumental in microstructural refinement, including grain refinement and increased dislocation density. The grain refinement of both the primary α-Al dendrites and the fibrous Si morphology is attributed to the high plastic strain that formed after LSP, increasing dislocation density and serving as a barrier to dislocation slip. This significantly enhanced the microhardness, yield strength (YS) and ultimate tensile strength (UTS) of the LSP-treated samples compared to the as-printed samples. The LSP also promoted the closure of surface defects, such as voids, pores, and microcracks, thereby further improving strength and ductility. Even though there was a slight decrease in ductility as a result of strain hardening effect, there is general improvement in the overall mechanical performance, especially regarding tensile strength and hardness, confirming LSP as a veritable strategy for SLMed A357, suitable for critical applications in aerospace and biomedical applications. The findings emphasises the potential of LSP as an effective technique for optimising the performance of SLM-fabricated metallic alloys, particularly for applications where surface properties and high mechanical integrity are of concern.

Acknowledgements

This work is funded under the Centre of Excellence (COE) Research Grant (RG) UTM Flagship COE/RG Grant Vot. 10G01. The authors acknowledge the Universiti Teknologi Malaysia for approving the funding, which made this research possible.

Author Contributions

All the authors in this study contributed towards the drafting, data analysis, and review of the work, and vouch to be accountable to the entire work.

Conflict of Interest

The authors declare no conflicts of interest regarding this study.

Compliance with Ethical Standards

This work is compliant with ethical standards.

References

[1] Rao, J. H., Zhang, Y., Fang, X., Chen, Y., Wu, X., and Davies, C. H. J. (2017). The origins fortensile properties of selective laser melted aluminium alloy A357. *Additive Manufacturing,* 17, 113-122.

[2] Es-Said, O., Lee, Pfost, O., Thompson, D., Patterson, D. L., Foyos, M., and Marloth, R. (2002)Alternative heat treatments for A357-T6 aluminum alloy," *Engineering Failure Analysis,* 9(1), 99-107.

[3] Dybowski, B., Adamczyk-Cieślak, B., Rodak, K., Bednarczyk, I., Kiełbus, A., and Mizera, J. (2015). The microstructure of AlSi7Mg alloy in as cast condition. *Solid state phenomena,* 229, 3-10.

[4] Fan, Z., Z., Li, J. L., and Li, S. S. (2012). Mechanism for mechanical properties of the A357 connection beam casting from solidification. *Applied Mechanics and Materials,* 217, 1762-1768.

[5] Alexopoulos, N. (2010). Impact properties of the aircraft cast aluminium alloy Al-7Si0. 6Mg (A357). In EPJ Web of Conferences, 6: EDP Sciences, 02002.

[6] Forn, A., Vaneetveld G., Pierret J. C., Menargues S., Baile M., Campillo M., and Rassili A. (2010). Thixoextrusion of A357 aluminium alloy. *Transactions of Nonferrous Metals Society of China,* 20, s1005-s1009.

[7] Loizaga, A., De la Fuente, E., Niklas, A., Barrenengoa, J., and Fernández-Calvo, A. (2010). Mechanical properties optimization of alloys AlSi7Mg casting in sand moulds. *Revista de Metalurgia,* 46, 64-70.

[8] Marterior, A. A. M., Nocheseda, C. J. C., and Balela, M. D. L. (2025). Effect of T6-like and T5-like Heat Treatment on the Microstructure and Hardness of Cast and 3D-Printed Al-Si-Mg Alloy Systems. *Philippine Journal of Science,* 154(1), 37-45.

[9] Xinlei, L., Qitang, H., Xiaochuan, M. and Li, F. (2014). Effect of centrifugal counter-gravity casting on solidification microstructure and mechanical properties of A357 aluminum alloy. *China Foundry,* 11(1).

[10] Cao, Y. Li, Lu, X., Bi, G., Song, Z., Li, X. and Fan, B. (2021). Effects of Casting Methods on Microstructure, Thermal Conductivity and Mechanical Properties of A356 Aluminum Alloy. *Special Casting & Nonferrous Alloys,* 41(11), 1424-1430.

[11] Rao, H., Giet, S., Yang, K., Wu, X., and Davies, C. H. (2016). The influence of processing parameters on aluminium alloy A357 manufactured by Selective Laser Melting. *Materials & Design,* 109, 334-346.

[12] Nasab, M. H., Vadani, M., Loge, R. E., Sohrabi, N., Jamili, A. M., Du Plesis, A. and Beretta, S. (2013). An investigation on the fatigue behavior of additively manufactured laser shock peened AlSi7Mg alloy surfaces. *Materials Characterization,* 200,112907.

[13] Zhao, Z., Li, L., Tan, L., Bai, P., Li, J., Wu, L. and Chen, Y. (2018). Simulation of stress field during the selective laser melting process of the nickel-based superalloy, GH4169. *Materials,* 11(9), 1525.

[14] Wang, M., Song, B., Wei, Q., Zhang, Y., and Shi, Y. (2019). Effects of annealing on the microstructure and mechanical properties of selective laser melted AlSi7Mg alloy. *Materials Science and Engineering: A,* 739, 463-472.

[15] Chen, Y., Sun, H., Li, Z. Z., Wu, Y., Xiao, Y., Chen, Z., and Wang, H. (2020). Strategy of residual stress determination on selective laser melted Al alloy using XRD. *Materials,* 13(2), 451.

[16] Chadwick, D. J., Ghanbari, S., Bahr, D. F., and Sangid, M. D. (2018). Crack incubation in shot peened AA7050 and mechanism for fatigue enhancement. *Fatigue & Fracture of Engineering Materials & Structures,* 41(1)71-83.

[17] Kalentics, N., Boillat, E., Peyre, P., Ćirić-Kostić, S., Bogojević, N., and Logé, R. E. (2017). Tailoring residual stress profile of selective laser melted parts by laser shock peening. *Additive Manufacturing,* 16, 90-97.

[18] Sandmann, P., Keller, S., Kashaev, N., Ghaouse, S., Hooper, P. A., Klusemann, B., and Davies, C. M. (2022). Influence of laser shock peening on the residual stresses in additively manufactured 316L by Laser Powder Bed Fusion: A combined experimental–numerical study. *Additive Manufacturing,* 60, 103204.

[19] Ramadas, H., Sarkar, S., Ganesh, P., Kaul, R., Majumdar, J. D., and Nath, A. K. (2023). Enhancing the static and dynamic mechanical properties of laser powder bed fusion process built 15–5precipitation hardening stainless steel specimens by laser shock peening. *Materials Science and Engineering: A,* 866, 144657.

[20] Vemanaboina, H., Padamurthy, A., Gandla, A. K., Muppa, L. R., and Lakshmi, K. K. (2024). Microstructure, wear and residual stresses of selective laser melting AlSi10Mg solid cylinder. *Proceedings of the Institution of Mechanical Engineers, Part E: Journal of Process Mechanical Engineering,* p. 09544089241272825.

[21] Hatamleh, M. I. (2019). Prediction of Residual Stress Random Fields in Selective Laser Melted Aluminum A357 Components Subjected to Laser Shock Peening. The University of Texas at Dallas.

[22] Hatamleh, M. I., Sadeh, S., Farooq, T., Malik, A. S., and Qian, D. (2018). Finite element study of laser peening on selective laser melted A357 aluminum alloy during tension test. in *International Manufacturing Science and Engineering Conference*, 2018, vol. 51388: American Society of Mechanical Engineers, V004T03A046.

[23] Hatamleh, M. I., Mahadevan, J., Malik, A., Qian, D., and Kovacevic, R. (2019). Prediction of residual stress random fields for selective laser melted A357 aluminum alloy subjected to laser shock peening. *Journal of Manufacturing Science and Engineering,* 141(10), 101011.

[24] Nasab, M. H., Romano, S., Gastaldi, D., Beretta, S., and Vedani, M. (2020). Combined effect of surface anomalies and volumetric defects on fatigue assessment of AlSi7Mg fabricated via laser powder bed fusion. *Additive Manufacturing,* 34, 100918.

[25] Montross, C. S., Wei, T., Ye, L., Clark, G., and Mai, Y. W. (2002). Laser shock processing and its effects on microstructure and properties of metal alloys: a review. *International journal of fatigue,* 24(10), 1021-1036.

[26] Thijs, L., Kempen, K., Kruth, J. P., and Van Humbeeck, J. (2013). Fine-structured aluminium products with controllable texture by selective laser melting of pre-alloyed AlSi10Mg powder. *Acta Materialia,* 61(5),1809-1819.

[27] Dhakal, B., and Swaroop, S. (2020). Effect of laser shock peening on mechanical and microstructural aspects of 6061-T6 aluminum alloy. *Journal of materials processing technology,* 282, 116640.

[28] Lan, L., Xin, R., Jin, X., Gao, S., He, B., Rong, Y., and Min, N. (2020). Effects of laser shock peening on microstructure and properties of Ti–6Al–4V titanium alloy fabricated via selective laser melting. *Materials,* 13(15), 3261.

[29] Mohd Noor, M., and Jamaludin, S. B. (3013). The Effects of Superheating Treatment on Distribution of Eutectic Silicon Particles in A357-Continuous Stainless Steel Composite. *Advanced Materials Research,* 620, 511-516.

[30] Du Plessis, A., Glaser, D., Moller, H., Mathe, N., Tshabalala, L., Mfusi, B., and Ostert, R. (2019). Pore closure effect of laser shock peening of additively manufactured AlSi10Mg. *3D Printing and Additive Manufacturing,* 6(5),245-252.